AN EXPLORATORY TWO-DIMENSIONAL STUDY OF THE COARSE STRUCTURE OF NETWORK MAGNETIC FIELDS

R. G. GIOVANELLI*

CSIRO Division of Applied Physics, P.O. Box 218, Lindfield, N.S.W. 2070, Australia

(Received 8 October, 1979; in revised form 28 March, 1980)

Abstract. Magnetograms in lines originating high in the solar atmosphere show, away from disk center, diffuse fringes of reverse polarity on the limbward side and diffuse centerwards extensions of normal polarity wherever the field is strong. Analysis of a Mg b_2 magnetogram reveals that, in active regions (and, hence, wherever the magnetic network is well developed) fields cover associated supergranules completely at heights mostly below 500–600 km (zero height is at $\tau_{5000} = 1$) but possibly up to 700–800 km at great distances (e.g. $>10^4$ km) from the network. These lie much lower than previously believed, mostly around the solar average temperature minimum. Near plagettes, the low-lying field has been measured out to ~6000–7000 km. One consequence is that in active regions and plagettes, the chromosphere-corona transition region probably penetrates below 600 km; another is that potential theory is inapplicable at coronal heights below about 15 000 km.

A more accurate analysis requires a specific atmospheric model for magnetic regions. Attention is drawn to the need for studying the consequences for acoustic wave propagation, reflection and dissipation in regions of strong network fields.

1. Introduction

Solar magnetograms are usually obtained in the wings of spectral lines having strong Zeeman splitting, e.g. Fe I 5233, 5250, 8688, Ca I 6103, etc. These wings originate at relatively low levels in the atmosphere where high-resolution magnetograms show the fields concentrated into tiny elements whose diameters, according to modern studies, are only some 100 km or so with field strengths 1000–2000 G. The elements are dotted quite irregularly along supergranule boundaries, being quite concentrated in plage regions and usually sparse elsewhere.

Kilogauss fields can be contained only deep in the atmosphere where the external gas pressure exceeds the magnetic pressure $B^2/8\pi$, a much weaker internal gas pressure ensuring pressure balance. Higher in the atmosphere, where gas pressures are lower, the flux tube comprising the magnetic element is expected to open out, a process which continues with height until interference occurs with fields originating in nearby elements. These are usually of the same polarity; and since the elements lie along the supergranule boundary, a more-or-less two-dimensional field should be produced whose regularity depends on the regularity of spacing of the elements. The field should continue to open out with height until interaction takes place with other fields originating on the opposite side of the supergranule or elsewhere, so forming a magnetic canopy over a non-magnetic region. Gabriel (1976) has given 1500 km as the typical height at which the canopy occurs, sufficiently high not to have any

* Visiting Astronomer, Kitt Peak National Observatory.†

† Operated by the Association of Universities for Research in Astronomy, Inc. under contract with the National Science Foundation.

Solar Physics **68** (1980) 49–69. 0038-0938/80/0681-0049$03.15.

significant impact on the physical properties of the photosphere or chromosphere until 1000 km above the temperature minimum, but no direct observational study has ever been made.

Indirect observational evidence of chromospheric fields comes from monochromatic images in Hα and a few other lines of high origin which show well-developed fibril structures wherever there are strong network fields. These are believed to lie along lines of force. Their vertical structures are best seen towards the limb in off-band Hα filtergrams such as obtained by Dunn (1971; reproduced in Athay 1974, 1976). Characteristically, they lie within 3000–4000 km from the network, extend 4000 to 5000 km out, and are curved but usually confined to angles within, say, 45° from the vertical. Their numbers are comparable with those of filigree points (which are coincident with the magnetic elements), but it has been impossible to establish whether individual fibrils come from individual filigree points. The *appearance* of fibrils towards the limb is of discrete structures lying in narrow, isolated tubes of force. They provide no hint of a field which should open out continuously to cover the neighboring supergranules at heights no greater than 1500 km at most.

There is really no intrinsic difficulty in recording magnetograms of higher levels than usual with strong lines such as Ca II 8542 or Mg I b_2, for many magnetograms in these and other lines have been obtained at Kitt Peak National Observatory (and, no doubt, elsewhere) over the past decade. They invariably show field expansion or bending.

This is illustrated clearly by two magnetograms obtained by W. C. Livingston on 12 March 1970, one of lower level in Fe I 5233, the other of higher level in Mg I b_2 (Figure 1). There are at least two intriguing differences between them:

(1) The 5233 Å line shows the typical characteristics of an active Sun. There are extensive unipolar regions where the fields are confined to (and outline) the supergranule boundaries (the network). In other regions, e.g. near disk center and elsewhere, the field is fragmentary. There are strong field concentrations in and near sunspots, but towards the W limb the b_2 line shows very obviously that the network fields, unipolar in 5233 Å, now appear bipolar with the reverse polarity always on the limbward side. This is so around much of the disk further than about 40–45° from disk center, particularly where the field concentration is greater. The phenomenon was first noticed by Chapman and Sheeley (1968) using an unstated line near the extreme limb, and described in somewhat more detail by Pope and Mosher (1975). Both groups of authors inferred that, on the limbward side, we are seeing lines of force which are inclined away from the observer. The phenomenon is not confined merely to the immediate neighborhood of the network; a comparison between the two magnetograms shows that, at least in plage regions, the reverse polarity is obvious, though falling off continuously, over distances of the order of a supergranule radius.

(2) The other difference between the magnetograms may be seen in b_2 nearer to disk center, and also towards the limb, wherever the fields appear strong. It is a

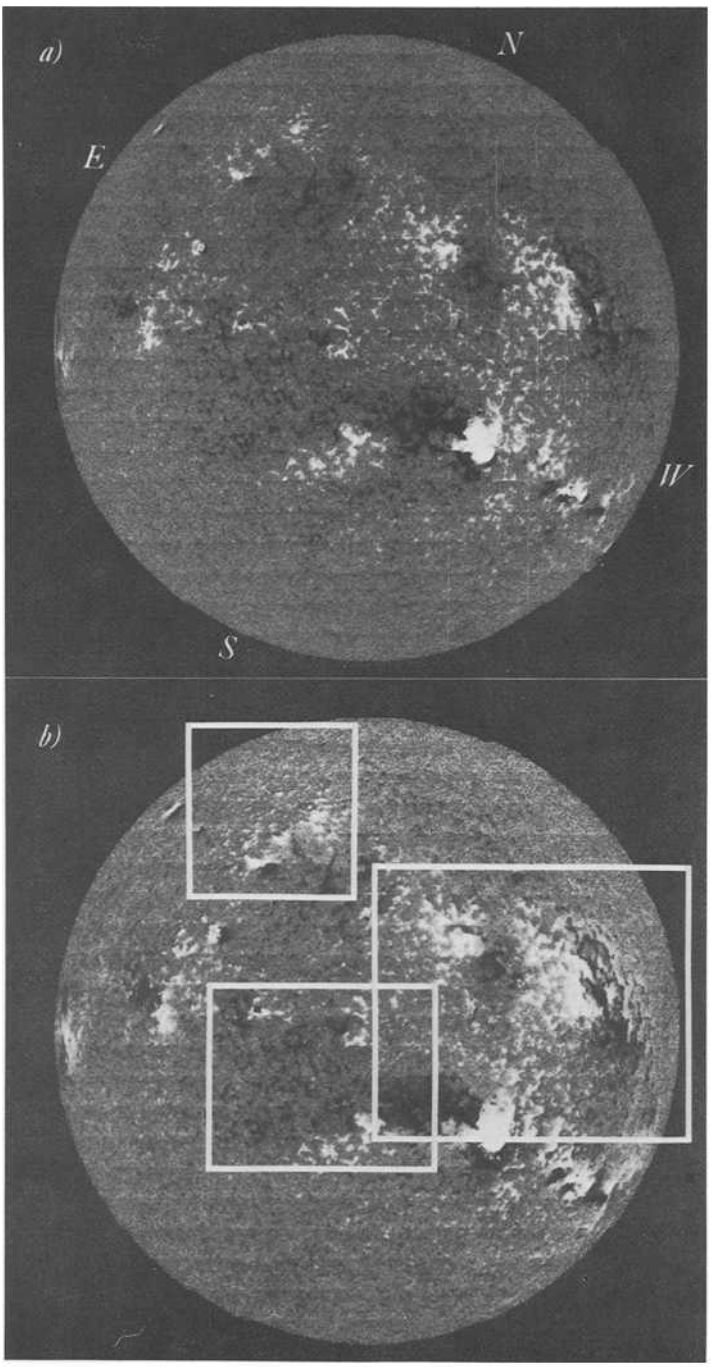

Fig. 1. Solar magnetograms for 12 March 1970. (a) Fe I 5233, (b) Mg I b_2 (5173 Å). In (b) the NW active region has very obvious diffuse fringes of reverse polarity on the limbward side of the dark-polarity network and centerwards diffuse extensions of normal polarity in the light-polarity network. Limbward reverse polarities are seen fringing isolated NE field fragments or plagettes. Numerous regions of smooth, diffuse field can be noted in (b) where none is seen in (a). These are all interpreted as due to fields expanding with height and forming extensive canopies over low field-free regions.

diffuse extension, towards disk center, of field of the same polarity over regions which are field-free in 5233 Å. Here, too, it appears that in b_2 we are seeing down to regions where the fields have opened out widely. Not all parts of the b_2 magnetogram show this extension; it is visible most readily at some 30–60° from disk center.

Magnetograms obtained in 1974 by Dr W. C. Livingston allow comparisons between several other lines – C I 9111, Fe I 8688, and Ca II 8542. The phenomena described above are absent in 9111 Å, which originates very low in the atmosphere, but present to differing extents in the intermediate 8688 Å and higher level 8542 Å lines.

The following section provides quantitative information on the variation of field strength recorded in b_2 across selected networks. Section 3 analyzes these results and derives the height at which the base of the field lies as function of distance from the network. It turns out that, in regions where the magnetic network is well developed, the field opens out and becomes virtually horizontal as low as 500–600 km above $\tau_c = 1$, very much lower than previous studies have suggested; above this level, the whole chromosphere is pervaded by field. In the Discussion, we show that the field opens out continuously rather than remaining in narrow tubes as in the fibrils, consider the reliability of the results, and list some of the consequences apparent immediately for various branches of solar physics.

2. The Measured Fields

2.1. Calibrations

The observations of 12 March 1970 were obtained with the 40-channel magnetograph and the McMath telescope. The same slits were used in both lines, extending 0.075 Å to 0.25 Å from line center in b_2 and effectively the same in 5233 Å. The grid spacing was approximately $2.35'' \times 2.35''$ both along and across the direction of scan. The magnetograph had been calibrated directly in 5233 Å (but not in b_2) by applying a uniform-field Zeeman splitting to the average center-of-disk line profile. In any case, direct calibrations in different lines are known to lead to different fluxes (Harvey and Livingston, 1969). Whatever the reasons, the best we can still do, even now, is to adopt the results from 5233 Å as standard, the b_2 calibration being fixed to achieve equal fluxes (on average) in 5233 Å and b_2 for a large number of identical networks near disk center. There is no obvious systematic variation with the strength of the network. All b_2 line-of-sight fields reported here (B_r) have been calibrated in this way.

2.2. Network reverse-polarities

The magnetic network is well developed only in active regions. Even so, network fields are far from regular. The supergranules, on whose boundaries the elements lie, are irregular in shape and size. The magnetic elements are distributed irregularly along the boundaries, so that the apparent width and strength of field vary greatly.

There are also isolated elements of both polarities in the cell interiors which cause fluctuations in the records of what might otherwise be uniform overlying fields.

To ease these problems, we have selected, as far as possible, network approximately parallel to the limb and of roughly uniform appearance, and extracted fields along approximately radial traverses. Averaging has been carried out after appropriate phase shifts to take account of irregularities in the network axis.

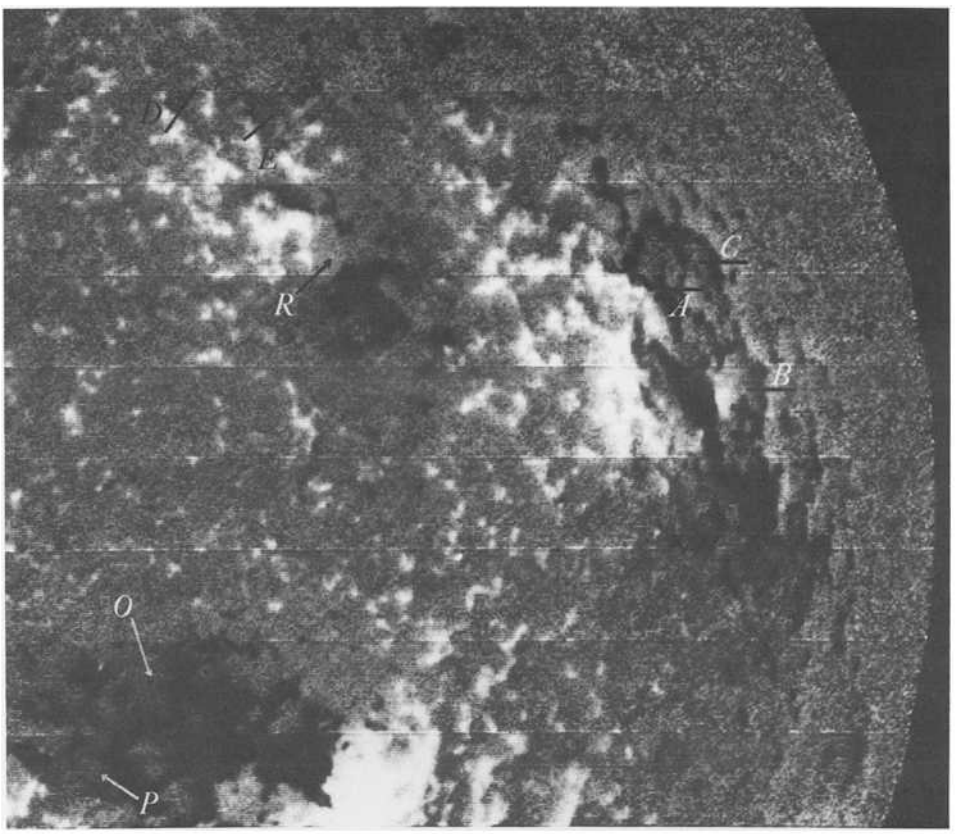

Fig. 2. NW region of Figure 1(b), enlarged.

Figure 2 is an enlargement of two NW active regions which exhibit extensive polarity reversals. In A, B, and C, the normal polarity is dark; in D and E, light. The mean variations in recorded field strength across these networks are plotted in Figure 5(a). Network A is somewhat irregular in that the normal network field (dark) is narrow at the northern end but, at the southern end, is adjacent to a rather extensive strong-field region. For this reason, the average normal field of A shown in Figure 5(a) is not necessarily a good representation of average b_2 field strengths in network of normal polarity. In network B, there are also rather large variations along the normal network. In C, the reverse field drops almost to zero and then rises again

closer to the limb, a behavior which is not observed in other networks, and we have extrapolated to zero the virtually-linear drop before the minimum.

In D, E, extensive reverse fields appear as close as 26° to disk center (it is rather difficult to see reverse polarities much closer than this). For D, in which the width of the region of reverse polarity varies considerably, we give separate average data for two different parts of the network (Figure 5(a)).

In the two NW active regions, there seems to be no place where fields are not recorded in b_2. The normal and reverse polarities are of approximately equal widths, the combined widths occupying about 5.2×10^4 and 5.9×10^4 km for the two parts of B, 4.2×10^4 km for C. The corresponding supergranule cells would be much larger than average; perhaps they represent pairs of cells whose common boundaries have no field.

Away from active regions, the field is fragmentary (plagettes), some examples being shown in Figure 3. Average fields effectively transverse to the network axis are given in Figure 5(b). The reverse fields are much smaller than the normal in magnitude and extent.

Over all, these graphs show the typical behaviour of network reverse fields. The changeover from normal to reverse polarity is invariably very sudden. The location of the transition point has been found by blink comparison of the 5233 Å and b_2

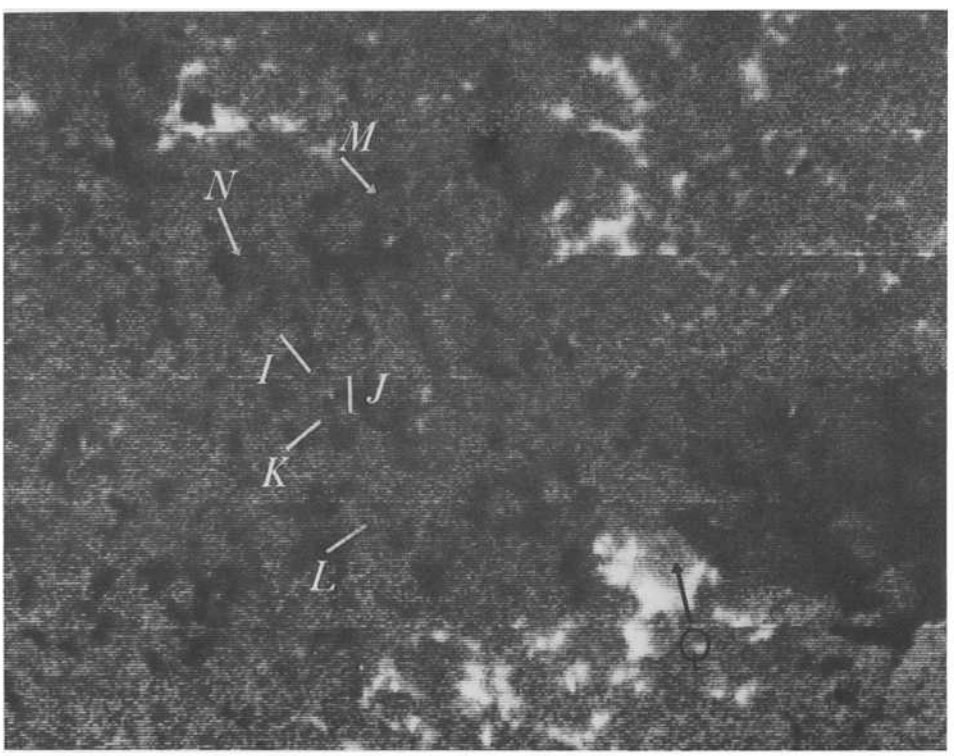

Fig. 3. NE region of Figure 1(b), enlarged.

magnetograms (despite the 6-hour time difference); to within the resolution limits, it lies immediately on (or above) the limbward edge of the unipolar network observed in 5233 Å. The uncertainty in this location is probably about on-half pixel for A, B, and C, some 1400 km at 50–55° from disk center; for D and E, where the transition is softer, the uncertainty is about 2000 km.

2.3. Diffuse unipolar fields

In Figure 3, I, J, K, L, M, and N are parts of a region which are unipolar in both 5233 Å and b_2; but in the former, the network is more compact and symmetrical, whereas in b_2 it is broader and asymmetric, with a diffuse extension usually, but not invariably, towards disk center (e.g. network I is aligned *towards* disk center and still has a sharp drop to zero on one side with a diffuse extension on the other). Even

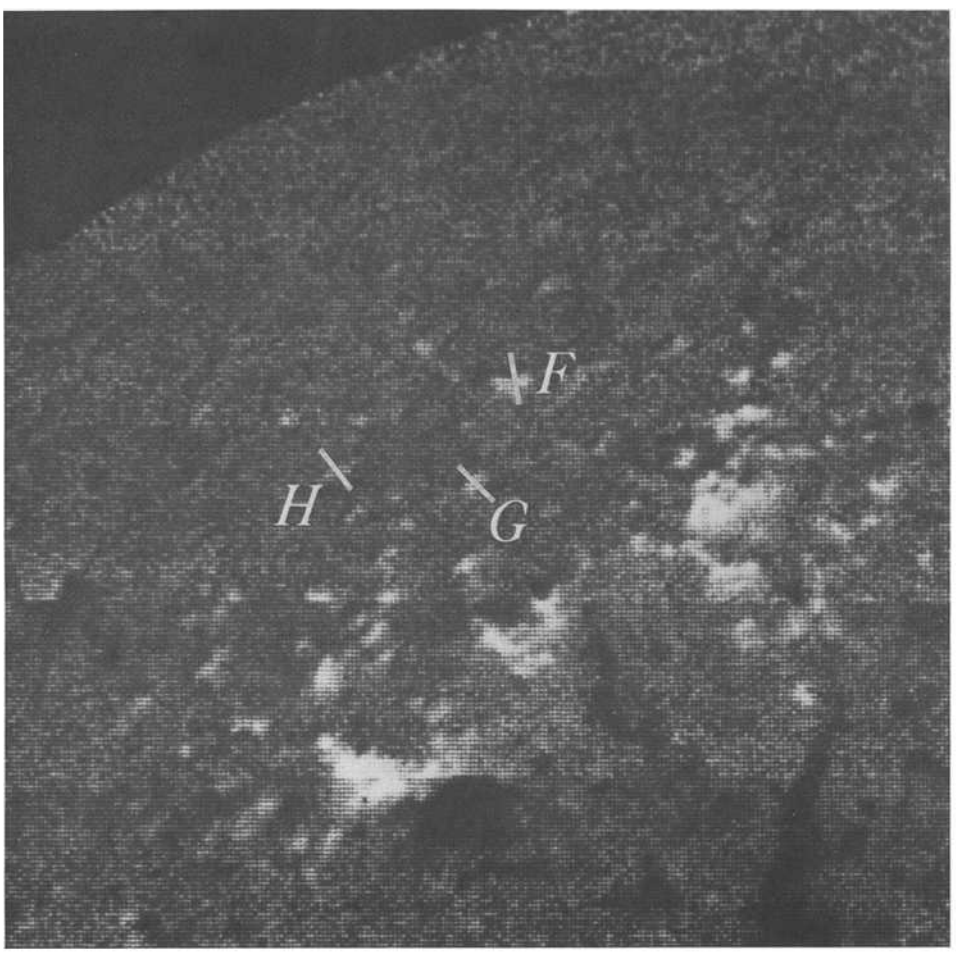

Fig. 4. Southern large-scale unipolar region (left) and active region (right) of Figure 1(b), enlarged.

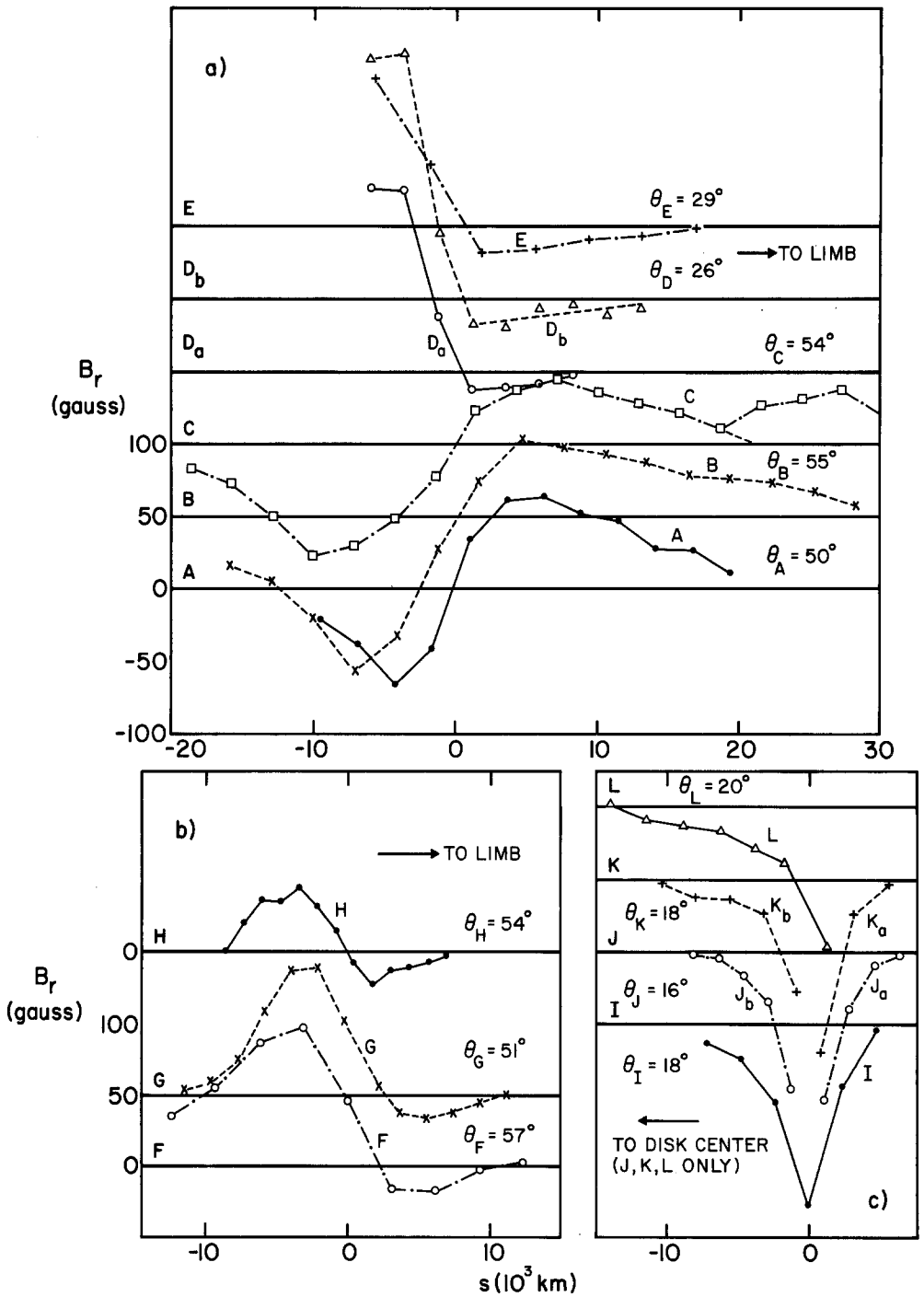

Fig. 5. Measured field variation across network boundaries in the b_2 line. All distances are along the surface of the Sun at right angles to the network axis. (a) Networks in Figure 2, (b) in Figure 3, (c) in Figure 4. The various graphs have separate zero levels as indicated.

more-striking diffuse unipolar extensions are to be seen in the region of light polarity in Figure 2.

It is more difficult to obtain representative data for these networks since there is no simple criterion (such as the transition point) on how to superimpose adjacent traces. Arbitrarily, we have taken the last point where the recorded field exceeds 62.5 G as at the edge of the network and then derived average fields at given distances away from the network. The averages for I, J, K, and L are shown in Figure 5(c).

The diffuse extensions of M and N are more irregular; for these, only the average overall line-of-sight fields have been derived; 13.1 G at typically 7000 km from the nearest network in M, and 11.3 G at typically 3500 km in N.

O and P are large, diffuse unipolar areas associated with the intense SW active region. Typically, $B_r = 10$ G in O, some 12° from disk center, and 20 G in P, some 16°.

2.4. Diffuse field joining networks of opposite polarities

Q is an interesting example of a diffuse b_2 field covering a large area of zero field strength in 5233 Å (no doubt a supergranule cell interior) separating networks of opposite polarities some 15° from disk center. The sharpness and sense of the polarity reversal are in conformity with the reverse-polarity networks much further from disk center (Section 2.2). However, the phenomenon is probably more complicated here, since a similar example R (Figure 2) in which B_r is typically 34 G shows the sharp field-reversal to be almost radial, if anything, in the opposite sense. For a satisfactory interpretation in such cases (and probably I, Section 2.3) we need more information on field alignment, such as may be obtainable from the orientations of chromospheric fibrils.

3. Analysis

We shall now show how these observations can yield the height of the boundary to the magnetic region, and its variation with distance from the network.

The observation of diffuse field in b_2 where none is present in the 5233 Å line originating lower in the atmosphere raises a new problem; the line of sight obviously passes through a region of substantial field into an effectively field-free region below. Therefore, the magnetograph signal will be lower than if the mean field of the upper region extended uniformly downwards. This phenomenon probably occurs to some extent for almost *all* magnetograph measurements except in sunspots.

To derive information on the field, we shall be assuming later that it is uniform in strength and direction above some height z_0 and zero below, but no such restrictive assumption is made initially.

3.1. Magnetograph response to a field which is non-uniform along the line of sight

Figure 6 shows the geometry involved, S being the photospheric level $\tau_c = 1$, and L the line of sight; the magnetic region is hatched, the non-magnetic clear. Consider

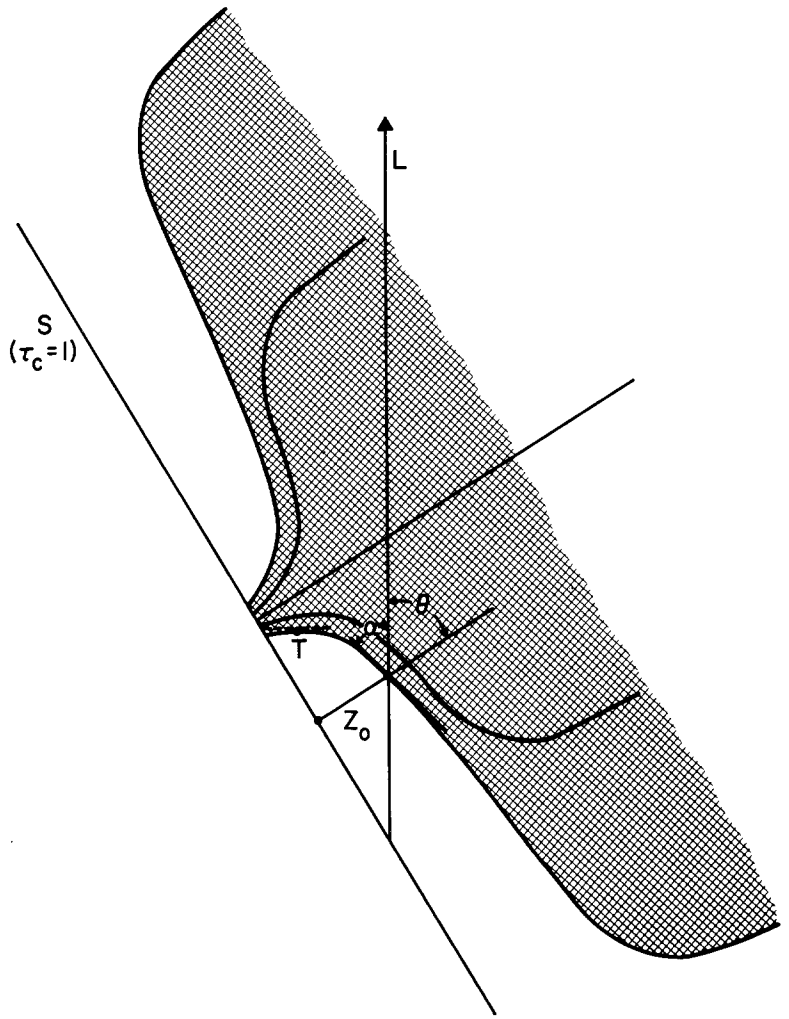

Fig. 6. Schematic diagram of the 2-dimensional field geometry at angle θ from disk center. The magnetic canopy is hatched, the non-magnetic region clear. L is the line of sight and S the level $\tau_c = 1$. The angle between the field boundary and the line of sight is α. At T, the transition between normal and reverse polarity, the tangent is effectively perpendicular to the line of sight.

first the formation of a spectral line in a one-dimensional atmosphere in the absence of a magnetic field. Let $\varepsilon_{\Delta\lambda}$ be the emissivity, $\kappa_{\Delta\lambda}$ the attenuation coefficient of the gas at $\Delta\lambda$ from the line center. Then the contribution from unit volume to the escaping intensity is $\varepsilon_{\Delta\lambda} \exp(-\tau_{\Delta\lambda}/\mu)$, where $\tau_{\Delta\lambda} = \int_z^\infty \kappa_{\Delta\lambda}\, dz$ is the optical depth at height z (positive outwards) and $\theta = \cos^{-1}\mu$ is the angle to the vertical. For simplicity, we shall suppose continuous absorption negligible in the part of the line used.

Now let there be a longitudinal magnetic field splitting the line by $\pm\Delta\lambda$, the emissivity in each component being $\frac{1}{2}\varepsilon_{\Delta\lambda\pm\Delta\lambda}$ where, here and elsewhere in this section, the upper or lower sign is to be used respectively with the blue- or red-shifted

component. The contribution of unit volume to the escaping intensity in each component is

$$\tfrac{1}{2}\varepsilon_{\Delta\Lambda\pm\Delta\lambda}\exp\left(-\tau_{\Delta\Lambda\pm\Delta\lambda}/\mu\right),$$

and the escaping intensity in each component is

$$I_{\Delta\Lambda\pm\Delta\lambda}=\tfrac{1}{2}\int_{-\infty}^{\infty}\varepsilon_{\Delta\Lambda\pm\Delta\lambda}\exp\left(-\tau_{\Delta\Lambda\pm\Delta\lambda}/\nu\right)\mathrm{d}z/\mu\,. \tag{3.1}$$

At $\Delta\Lambda$, the difference between the two components is

$$\Delta I_{\Delta\Lambda}=\tfrac{1}{2}\int_{-\infty}^{\infty}\varepsilon_{\Delta\Lambda+\Delta\lambda}\exp\left(-\tau_{\Delta\Lambda+\Delta\lambda}/\mu\right)\mathrm{d}z/\mu-$$

$$-\tfrac{1}{2}\int_{-\infty}^{\infty}\varepsilon_{\Delta\Lambda-\Delta\lambda}\exp\left(-\tau_{\Delta\Lambda-\Delta\lambda}/\mu\right)\mathrm{d}z/\mu\,.$$

We suppose that $\Delta\lambda$ is small, so that

$$\varepsilon_{\Delta\Lambda\pm\Delta\lambda}=\varepsilon_{\Delta\Lambda}\pm\frac{\partial\varepsilon}{\partial\lambda}\Delta\lambda\,,$$

$$\tau_{\Delta\Lambda\pm\Delta\lambda}=\tau_{\Delta\Lambda}\pm\frac{\partial\tau}{\partial\lambda}\Delta\lambda\,.$$

Then

$$\exp\left(-\tau_{\Delta\Lambda\pm\Delta\lambda}/\mu\right)=\left(1\mp\frac{\partial\tau}{\partial\lambda}\frac{\Delta\lambda}{\mu}\right)\exp\left(-\tau_{\Delta\Lambda}/\mu\right)$$

and so

$$\Delta I=\tfrac{1}{2}\int_{-\infty}^{\infty}\left(\varepsilon_{\Delta\Lambda}+\frac{\partial\varepsilon}{\partial\lambda}\Delta\lambda\right)\left(1-\frac{\partial\tau}{\partial\lambda}\frac{\Delta\lambda}{\mu}\right)\exp\left(-\tau_{\Delta\Lambda}/\mu\right)\mathrm{d}z/\mu-$$

$$-\tfrac{1}{2}\int_{-\infty}^{\infty}\left(\varepsilon_{\Delta\Lambda}-\frac{\partial\varepsilon}{\partial\lambda}\Delta\lambda\right)\left(1+\frac{\partial\tau}{\partial\lambda}\frac{\Delta\lambda}{\mu}\right)\exp\left(-\tau_{\Delta\Lambda}/\mu\right)\mathrm{d}z/\mu=$$

$$=\int_{-\infty}^{\infty}\left(\frac{\partial\varepsilon}{\partial\lambda}\Delta\lambda-\varepsilon\frac{\partial\tau}{\partial\lambda}\frac{\Delta\lambda}{\mu}\right)\exp\left(-\tau/\mu\right)\mathrm{d}z/\mu\,, \tag{3.2}$$

where we have now dropped the subscript $\Delta\Lambda$ from ΔI, ε and τ. The difference in fluxes admittd by a monochromator in the range $\Delta\Lambda$ to $\Delta\Lambda+\delta\Lambda$, supposed to be of

uniform transmission throughout, is then

$$F = \int_{\Delta\Lambda}^{\Delta\Lambda+\delta\Lambda} \Delta I \, \mathrm{d}\lambda \,. \tag{3.3}$$

In the case of a magnetograph, F is proportional to the magnetograph signal.

Where a magnetic field is opening out with height, the field strength B is zero below the boundary, whose height z_0 may vary with distance from the network axis. At great heights, the field becomes more-or-less vertical and uniform, so that the effective field (the line-of-sight component) will be quite variable. For simplicity, we now adopt a model in which, along a line of sight, the field (and hence $\Delta\lambda$) is uniform above z_0 and zero below.

In such a case, the magnetograph response is proportional to F_0, where

$$F_0 = \int_{\Delta\Lambda}^{\Delta\Lambda+\delta\Lambda} \Delta\lambda \Big[\int_{z_0}^{\infty} \frac{\partial\varepsilon}{\partial\lambda} \exp(-\tau/\mu) - \int_{z_0}^{\infty} \frac{\varepsilon}{\mu} \frac{\partial\tau}{\partial\lambda} \exp(-\tau/\mu) - \int_{-\infty}^{z_0} \frac{\varepsilon}{\mu} \frac{\partial\tau_0}{\partial\lambda} \exp(-\tau/\mu) \Big] (\mathrm{d}z/\mu) \, \mathrm{d}\lambda$$

and $\tau_0 = \int_{z_0}^{\infty} \kappa_{\Delta\Lambda} \, \mathrm{d}z$. But in terms of the contribution function

$$C = \frac{\varepsilon}{\mu} \exp(-\tau/\mu),$$

$$\mu \frac{\partial C}{\partial\lambda} = \frac{\partial\varepsilon}{\partial\lambda} \exp(-\tau/\mu) - \frac{\varepsilon}{\mu} \frac{\partial\tau}{\partial\lambda} \exp(-\tau/\mu) \,.$$

So

$$F_0 = \Delta\lambda \int_{\Delta\Lambda}^{\Delta\Lambda+\delta\Lambda} \Big[\int_{z_0}^{\infty} \mu \frac{\partial C}{\partial\lambda} - \int_{-\infty}^{z_0} C \frac{\partial\tau_0}{\partial\lambda} \Big] (\mathrm{d}z/\mu) \mathrm{d}\lambda$$

$$= \Delta\lambda \int_{z_0}^{\infty} (C_{\Delta\Lambda+\delta\Lambda} - C_{\Delta\Lambda}) \, \mathrm{d}z - \frac{\Delta\lambda}{\mu} \int_{\Delta\Lambda}^{\Delta\Lambda+\delta\Lambda} \frac{\partial\tau_0}{\partial\lambda} \Big(\int_{-\infty}^{z_0} C \, \mathrm{d}z \Big) \mathrm{d}\lambda \,. \tag{3.4}$$

The value of F_0 may be derived numerically if the contribution function is known as a function of depth. In particular, if the field is uniform throughout the atmosphere,

$$F_\infty = \Delta\lambda \int_{-\infty}^{\infty} (C_{\Delta\Lambda+\delta\Lambda} - C_{\Delta\Lambda}) \, \mathrm{d}z \,. \tag{3.5}$$

This is the condition for which the magnetograph is calibrated. Thus if the magnetograph reading is B_r and the field is uniform above z_0, zero below, the line-of-sight component of the field is B_r/F_z, where $F_z = F_0/F_\infty$.

But there are still difficulties in calculating F_z, for the contribution functions need to be based on an atmospheric model, whereas a reliable magnetic-region model based preferably on continuum data still seems to be lacking. The pressure is substantially lower in a magnetic flux tube than for the same z in its non-magnetic surroundings and the temperature (or excitation temperature) is unknown. To make progress, it is necessary to assume (effectively as in the case of all other magnetograph measurements) that the F_z calculated with a standard atmospheric model apply well enough for present purposes.

Dr H. Jones has kindly undertaken and supplied preliminary calculations, based effectively on the HSRA, of F_z for the b_2 line with slits extending from $\Delta\Lambda = 0.075$ Å to $\Delta\Lambda + \delta\Lambda = 0.25$ Å for $\mu = 1, 0.7$, and 0.5. The general trends are the same for all μ, and we use those for $\mu = 0.5$ for all the following analyses. F_z is near unity up to 200 km, falls to ~ 0.5 by 400 km as the optical depth throughout the range transmitted by the monochromator drops below unity, and then falls more slowly with height (Table I).

TABLE I

Height variation of F_z, for $\mu = 0.5$, and B_{max} (HRSA)

Height (km)	$F_z(b_2)$, $\mu = 0.5$	B_{max}(gauss)	$B_{max}F_z$
0	1.00	1821	1821
100	1.00	1245	1245
200	0.99	813	805
300	0.78	521	406
400	0.48	324	156
500	0.34	197	67
600	0.27	116	31
700	0.215	72.5	15.6
800	0.155	49.0	7.6
900	0.100	32.0	3.2
1000	0.070	21.4	1.5

3.2. Field strength at the field boundary

At the boundary of the magnetic field where it sweeps over the nonmagnetic atmosphere, the condition of pressure balance applies:

$$p_e - p_i = B^2/8\pi,$$

where p_e, p_i are the gas pressures immediately outside in the field-free region and immediately adjacent within the field. The maximum possible equilibrium field at the boundary is thus

$$B_{max} = (8\pi p_e)^{1/2}. \tag{3.6}$$

Values of B_{max} and of $B_{max}F_z$ are also listed in Table I against height in the HSRA. With these, we can readily place limits on z_0; for the recorded field, B_r cannot exceed $B_{max}F_z \cos \alpha$, where α is the angle between the field and the line of sight, i.e.,

$$B_{max}F_z \geq B_r/\cos \alpha \,. \tag{3.7}$$

All that is now required is to estimate α, and this we do in the following subsection.

3.3. Results

Along the line of sight to the transition point between normal and reverse fields, the weighted mean field is perpendicular to the line of sight. Therefore, in network parallel to the limb, the tangent to the boundary at the transition point T (Figure 6) must be inclined to the horizontal at an angle close to θ, the angle from the center of the disk. We have seen that this occurs in active regions within, at most, 1400 km from the 5233 Å network.

Further from the network, the lines of force must be inclined even further from the vertical, ultimately becoming almost horizontal. For network parallel to the limb and approximately radial field lines, as in most cases studied here,

$$\alpha \geq \frac{\pi}{2} - \theta \,. \tag{3.8}$$

By putting $\alpha = (\pi/2) - \theta$ and using the measured value B_r in (3.7), we derive a *lower limit* for $B_{max}F_z$ which, by comparison with the values listed in Table I, leads to an upper limit for z_0, the height of the field boundary above $\tau_c = 1$.

An example illustrates the technique. In network A, $B_r = 52$ G in the reverse field some 8900 km from the transition point. Since $\theta = 54°$, $z_0 \leq 500$ km.

Figure 7(a) shows plots of upper limits to z_0 with distance from the transition point in the various active-region networks. Over a great deal of the range, the fields extend down to below 600 km. Any rise towards the network, e.g. in A, B, is due to errors in taking α to equal $(\pi/2) - \theta$, but the rise away from the network cannot be due to this.

Figure 7(b) shows similar plots for the reverse 'plagette' fields. They show no extended region of such low z_0, but the upper limits are still typically only 600–700 km out to 4000 km.

Figure 7(c) contains plots for the large-scale unipolar region. Network I is aligned towards disk center, but shows a diffuse extension on one side and none on the other. Clearly, the fields are asymmetric, and probably skew, so that $\alpha \ll (\pi/2) - \theta$, and $B_{max}F_z \gg B_r/\sin 18°$. Graph I shows the upper limits to z_0 so derived for the diffuse extension. Network J is aligned more towards the limb, and the upper limits to z_0 are shown for the extension towards disk center (J_b). A similar graph is given for K_b. Particularly with K, it is difficult to understand the sharpness of the network on the

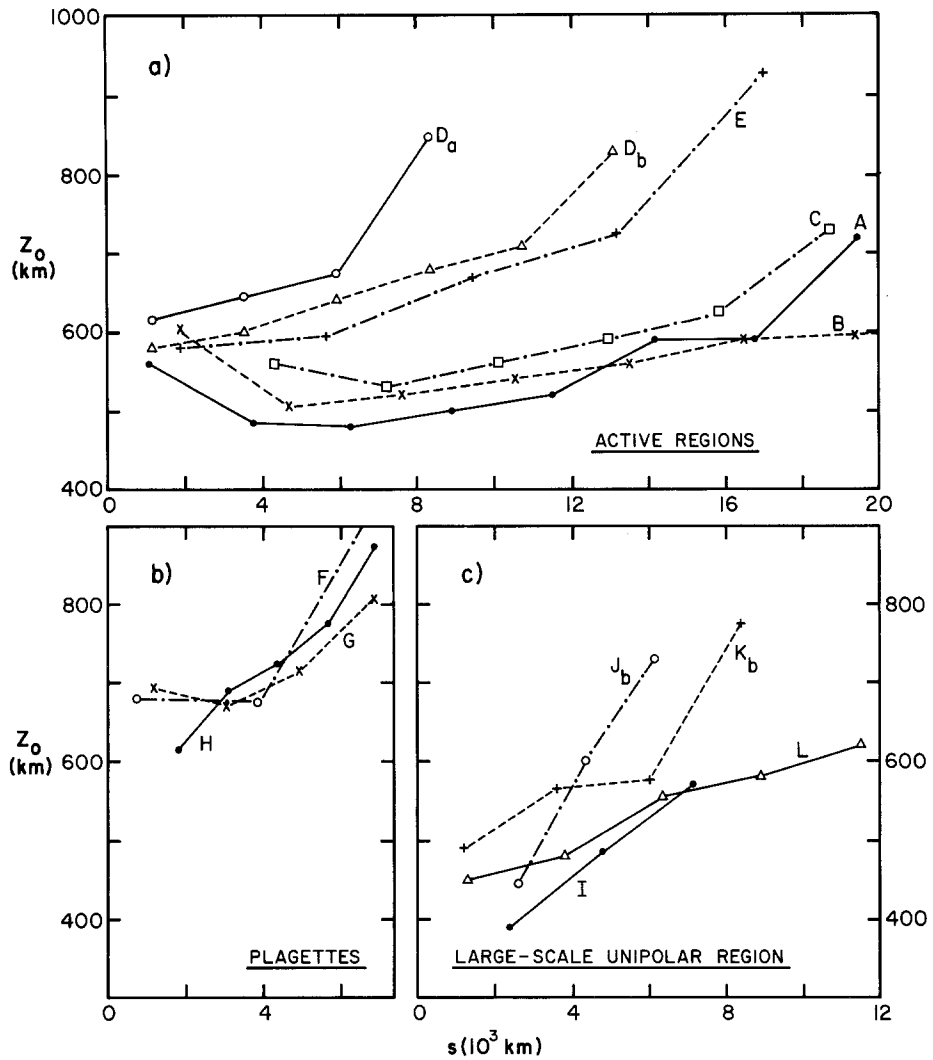

Fig. 7. Upper limits to height of lower boundary of field in individual networks, as functions of distance from the transition point (a, b) or network (c). (a) Networks in Figure 2, (b) in Figure 3, (c) in Figure 4.

limb side unless the field is asymmetric or skew. Network L exhibits an extension for which the upper limit to z_0 is $\lesssim$600 km out to 11 000 km from the 5233 Å network.

The other networks studied in this large-scale unipolar region, M, N, are rather irregular. While the field direction is uncertain, once more $\alpha \lesssim (\pi/2) - \theta$. Then upper limits to z_0 become 510 km at typically 7000 km from the nearest network in M, and 580 km at typically 3500 km from the nearest network in N.

Extensions from the intense active region at 0 and P have upper limits to z_0 of about 550 km and 500 km. For R, where the diffuse extension connects networks of opposite polarities, the upper limit to z_0 is typically 490 km.

4. Discussion

4.1. Reliability

The methods used here have been approximate, and in some aspects, based on assumptions that we would prefer to avoid, but there seems to be no better alternative at present. It has been necessary to use a model of line formation where source function and attenuation coefficient are the same inside the field as in the standard atmospheric model. But standard models are based on observations which do not resolve between but include both non-magnetic and magnetic regions. This is completely acceptable for the photosphere but may lead to significant errors higher; for the gas pressure is appreciably smaller in the magnetic regions, and these may occupy a significant fraction of the higher atmosphere. Even so, it is not clear whether, for any given spectral line, F_z would be reduced or increased by a more-realistic model applicable specifically to the magnetic regions.

The maximum possible error will have been made if, in the spectral range transmitted by the monochromator ($\Delta\lambda = 0.075$ to 0.25 Å), the b_2 lines were formed fully within the magnetic region. In this extreme case, F_z would be unity for all z, and $B_{\max} = B_r/\cos\alpha$. A comparison of $B_{\max}$ and the $B_{\max}F_z$ in Table I shows that height z_0 in Figure 7 would then be increased to Z_0 as follows:

z_0(km)	400	500	600	700	800
Z_0(km)	550	670	770	850	910.

These higher magnetic canopies are exceedingly unlikely, for they require optical depths of the order of unity, at heights of characteristically 700 km or more, out to 0.25 Å from line center; whereas even at the inner edge of the monochrometer slit, the optical depth is only ~0.1 at this height in the HSRA. The changes necessitated by a reliable model for a magnetic atmosphere may decrease or increase z_0; if the latter, the increases are likely to be small compared with the above extremes.

The analysis has been carried out ignoring fine-structure, but filtergrams of the chromosphere in lines from higher levels show that the regions influenced by magnetic fields are strongly fibrous in absorption and emission properties. However, spectroheliograms in b_2 examined by the author show no obvious fibrous structure, and we can be reasonably satisfied that such structures are unlikely to affect the results.

The magnetograph calibration is an embarrassing potential source of error. Differences in fluxes measured in different spectral lines (Harvey and Livingston, 1969) have been attributed to unresolved variations in line profile from non-magnetic to magnetic regions. While this is undoubtedly so in part, we have seen that non-uniformities in field have a major effect on F_z in the b_2 line. There must be analogous functions for the lines used more commonly for magnetic measurements. But the magnetic elements are much smaller than the resolution limit of the magnetograph, which integrates over a field having a widely varying lower boundary

(particularly along inclined lines of sight); so that lines originating at different levels, and having differing contribution functions, will be affected differently. This is a second factor contributing to the differences found by Livingston and Harvey. Because of it, the above use of 5233 Å to calibrate b_2 is a palliative not as reliable as the author would like.

4.2. Generality of the Results

Despite these difficulties, it is immediately apparent that, in active regions, i.e., where the magnetic network is well developed, magnetic fields cover the interiors of supergranule cells at heights of the order of 500–600 km or less. This holds also over quite a large fraction of the large-scale unipolar regions such as on the left-hand side of Figure 1, where the network is incomplete or fragmentary.

To help in generalizing these results, measurements of the flux per unit length of network have been made in the 5233 Å line for some of these regions:

Active regions: networks B, C: $1.5\text{–}3\times10^{11}$ Mx cm^{-1}.

Plagettes: networks F, G, H: $0.5\text{–}1\times10^{11}$ Mx cm^{-1}.

For comparison, the average flux per unit length of supergranule boundary (network not being distinguishable) has been measured in Fe 8688 in quiet regions close to disk center on 5 days in November 1978 and February 1979, the mean being 1×10^{10} Mx cm^{-1} (near sunspot minimum the fields may well be weaker).

The area covered by active regions can be measured only subjectively. The author's estimate for 12 March 1970 is about 20% of the disk, about an additional 30% being covered by large-scale unipolar magnetic regions. Even if somewhat overestimated, the consequent area of surface covered by low-lying fields is substantial.

No measurements of z_0 have been possible for very weak network fields; presumably z_0 is much higher in such cases.

In summary, the field of all well-developed magnetic cells opens out at low levels as described above. This conclusion applies also to the majority of the flux emerging from the photosphere in the active Sun. The heights involved are much lower than generally accepted hitherto.

4.3. Upward Extension of the Field

(1) *Another height limit.* One can calculate easily an upper limit to which field-free gas could extend in an array of uniform, unipolar supergranules of effective diameters $d = 3\times10^4$ km. If the flux per unit length of boundary be F, then at great heights where the field is uniform, its strength is

$$B_c = \tfrac{1}{2}F\pi d/\tfrac{1}{4}\pi d^2 = 2F/d$$

$$= 100\text{ G} \quad (F = 1.5\times10^{11}\text{ Mx cm}^{-1}),$$

$$= 6.6\text{ G} \quad (F = 10^{10}\text{ Mx cm}^{-1}).$$

These two cases correspond respectively to an active and a weak-field region.

In such a model, the field above the canopy is nowhere less than B_c, so that the highest point on the canopy (at the center of the supergranule) does not exceed z_m where $p_e \geq B_c^2/8\pi$ (depending on p_i). Thus

$$z_0 \leq z_m \leq 650 \text{ km} \quad (F = 1.5 \times 10^{11} \text{ Mx cm}^{-1}),$$
$$\leq 1350 \text{ km} \quad (F = 10^{10} \text{ Mx cm}^{-1}).$$

The upper limits to z_0 found from observation (Figure 7) fall mostly below these extremes.

Figure 8 shows the cross section of a uniform unipolar supergranule. In the small height range between the base of the canopy z_0 and z_m, the field is mainly horizontal, and any steady gas motions there will be mainly horizontal. Above z_m, the field turns mainly outwards.

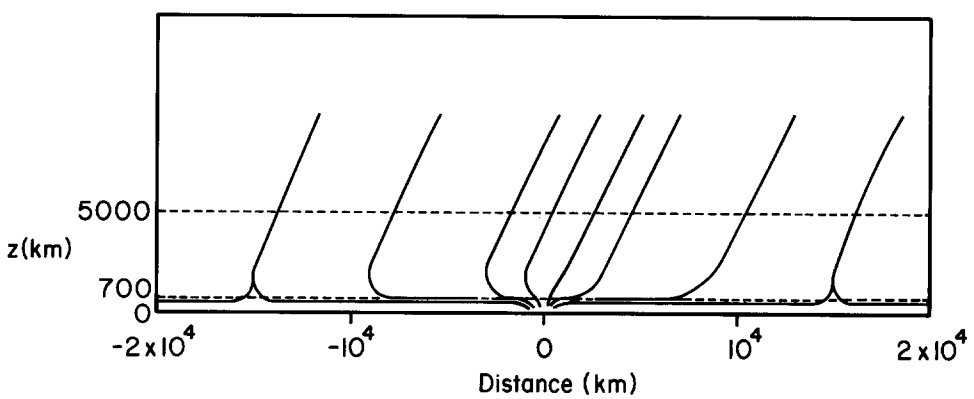

Fig. 8. Inferred typical field configuration across well-developed network (most outer field lines are omitted for clarity; the outward field should be uniform). The field forms a canopy over the non-magnetic regions at heights of 500–600 km or less. Off-band Hα fibrils are visible only at greater heights, e.g., in regions between the broken horizontal lines. Near the network, the field lines have shapes similar to the fibrils, which presumably mark particular field lines along which, for unknown reasons, density or excitation are high.

When neighboring networks are of opposite polarities (e.g., Q, Figure 3; R, Figure 2) the field must have a quite different character, resulting in fascinating Hα fibril structures. The field cannot be discussed adequately in the absence of corresponding fibril observations such as are needed to give field directions.

(2) *Relation to fibrils in unipolar supergranules.* The observations and analysis can be used to decide whether the field in the chromosphere is continuous or localized in the fibrils. Figure 1 and its enlargements show that the field extends outwards on both sides of the network, its base being almost exactly horizontal in most of the networks graphed in Figure 7. The line-of-sight components of the field pass effectively continuously from 'positive' to 'negative' near the centers of well-developed unipolar networks. Because of the interaction of fields from opposite sides

of the network, the lines of force must then bend upwards over the whole supergranule. This is contrary to what one sees in off-band Hα fibrils of well-formed network towards the limb, which are more-or-less confined to the neighborhood of the network. Therefore, extensive field is present over wide regions on both sides of the network where the fibrils discussed above are *not* observed. The field is not localized in the fibrils, and the fibrils do not give direct information on the process of field expansion, which seems to take place in at least qualitative agreement with theoretical expectations.

Then how do these fibrils fit into the picture? Their height range is from about 700 km or so to 5000 km or more. The important lower limit is uncertain observationally (about 1 arc sec) but Hα absorption becomes negligible towards the temperature minimum (Schoolman (1972) assesses the contribution function as negligible between 200 and 700 km) so that fibrils lie *above* the region of rapid expansion with height and so of almost horizontal field lines; there may be some additional explanation, but this is a sufficient reason for our inability to link fibrils to individual filigree points. Figure 8 (in which some of the outer field lines have been suppressed) shows that, above about 700 km, the field lines have the characteristic shapes of the fibrils in Dunn's (1971) picture. That the fibrils appear as isolated entities must be due to nonuniformities (of unknown origin) in excitation or density between different lines of force; we do not yet know the field strengths in fibrils, and they may well be regions of lower field strength and higher gas pressure than their surroundings.

4.4. Impact on Solar Physics

(1) *Atmospheric models.* The need for a specific atmospheric model for magnetic regions has been stressed in Section 4.1. But recognition of the extent to which active regions are overlain by field opens up the possibilities of being able to make appropriate measurements leading to such a model. The requirements are spatially-resolved spectral energy distributions in active regions with particular reference to the 0.125–0.2μ and 100–500μ ranges, which originate near or above the temperature minimum.*

There is an added bonus for an atmospheric model of a magnetic region; for the gases inside the field at greater heights are related hydrostatically to those inside the magnetic elements, so that we can see the possibility of improving greatly our information on physical conditions inside the elements.

(2) *Wave-propagation and atmospheric-heating mechanisms.* Virtually all studies of chromospheric heating assume this due to the dissipation of acoustic waves. The situation is changed dramatically in regions where there is a coverage of field at low levels. The waves that propagate there now become magnetodynamic, and the dissipation mechanisms need re-examination.

* Dr E. Avrett advises that models for various types of magnetic atmosphere will be published shortly in *Astrophys. J. Suppl.* by J. E. Vernazza, E. H. Avrett, and R. Loeser.

Wave reflection is also modified; reflection by the canopy of field becomes mixed in with reflection from the temperature minimum.

(3) *Chromosphere-corona transition region.* The low heights at which the field opens out imply that, in strong magnetic regions, the chromosphere-corona transition region penetrates deeply into the atmosphere. Accounts of network appearances in transition-region lines have related primarily to quiet regions (e.g. Reeves, 1976) where the network appears unchanged up to temperatures of some 3×10^5 K but effectively disappears before 1.4×10^6 K. If the same thing happens in active regions or even large-scale unipolar regions, it follows that, along most lines of sight, the base of the transition region lies no further than about 2 or 3×10^3 km from the network axis, depending on resolution. As may be seen from Figure 8, this requires in turn that, on most of the lines of force which, in the corona, are further than this from the axial field line, the transition region penetrates to near or below 600 km (Feldman *et al.*, 1979, have pointed out that the transition zone itself is highly inhomogeneous).

(4) *Fields derived from potential theory.* Many studies have been based on potential fields expected above the observed photospheric fields. The present work shows that potential theory is inapplicable in the chromosphere, but it should become valid at heights in the corona beyond about a supergranule radius, i.e. 15 000 km.

5. Summary

Magnetograms in lines originating high in the atmosphere show that, away from disk center, active regions and plagettes exhibit diffuse fringes of reverse polarity on the limbward side and diffuse centerwards extensions of normal polarity (Figure 1). These are interpreted as due to the fields opening out with height. The analysis of a b_2 magnetogram shows that, in active regions, the fields cover supergranules completely at heights mostly below 500–600 km (zero height being at $\tau_c = 1$), but with heights possibly up to 700 or 800 km at great distances from the network (Figure 7); these levels are much lower than the characteristic 1500 km usually accepted. For plagettes, the low-lying canopy is not measurable beyond typically 6000–7000 km from the network. The fields permeate the chromosphere fully above the level of the average temperature minimum.

The conclusions depend, in part, on the application of a plane-parallel model atmosphere such as HSRA, and emphasize once again the need to establish models more applicable to magnetic regions. They also make desirable an examination of the effects of the field canopy on the upward propagation of acoustic waves and on wave dissipation.

One consequence of the conclusions is that in active regions and plagettes, the chromosphere-corona transition region penetrates below the 600 km level. It is also clear that potential theory does not apply until above about 15 000 km.

Acknowledgements

My grateful thanks are due to Dr W. C. Livingston who drew my attention to the phenomenon and made his observations available for study. Dr H. Jones has kindly made available preliminary calculations of the function F_z required for the analysis. Thanks are also given to the Director, Kitt Peak National Observatory, who made the Observatory's facilities available and provided financial support for this investigation.

References

Athay, R. G. (ed.): 1974, 'Chromospheric Fine Structure', *IAU Symp.* **56**, 6.
Athay, R. G.: 1976, *The Solar Chromosphere and Corona: Quiet Sun*, D. Reidel Publ. Co., Dordrecht, Holland, p. 53.
Chapman, G. A. and Sheeley, N. R.: 1968, in K. O. Kiepenheuer (ed.), 'Structure and Development of Solar Active Regions', *IAU Symp.* **35**, 161.
Dunn, R. B.: 1971, *NBS Special Publication No. 353* (Menzel Symposium), p. 71.
Feldman, U., Doschek, G. A., and Mariska, J. T.: 1979, *Astrophys. J.* **229**, 369.
Gabriel, A. H.: 1976, *Phil. Trans. Roy. Soc.* **A281**, 339.
Harvey, J. W. and Livingston, W. C.: 1969, *Solar Phys.* **10**, 283.
Pope, T. and Mosher, J.: 1975, *Solar Phys.* **44**, 3.
Reeves, E. M.: 1976, *Solar Phys.* **46**, 53.
Schoolman, S. A.: 1972, *Solar Phys.* **22**, 344.